Appl Compos Mater (2012) 19:1–19
DOI 10.1007/s10443-010-9176-5

Numerical Study on Hybrid Tubes Subjected to Static and Dynamic Loading

M. Y. Huang · Yuh-Shiou Tai · H. T. Hu

Received: 2 August 2010 / Accepted: 13 October 2010 / Published online: 6 November 2010

Abstract The commercial finite element program LS-DYNA was employed to evaluate the response and energy absorbing capacity of cylindrical metal tubes that are externally wrapped with composite. The numerical simulation elucidated the crushing behaviors of these tubes under both quasi-static compression and axial dynamic impact loading. The effects of composite wall thickness, loading conditions and fiber ply orientation were examined. The stress–strain curves under different strain rates were used to determine the dynamic impact of strain rate effects on the metal. The results were compared with those of a simplified analytical model and the mean crushing force thus predicted agreed closely with the numerical simulations. The numerical results demonstrate that a wrapped composite can be utilized effectively to enhance the crushing characteristics and energy absorbing capacity of the tubes. Increasing the thickness of the composite increases the mean force and the specific energy absorption under both static and dynamic crushing. The ply pattern affects the energy absorption capacity and the failure mode of the metal tube and the composite material property is also significant in determining energy absorption efficiency.

Keywords Fiber-reinforced metal tubes · Energy absorption · Axial crushing · Impact loading · Specific energy absorption

1 Introduction

Numerous practical engineering systems must absorb various amounts of energy during impact events. In recently years, fiber composite materials have been increasingly used in the development of advanced metal shell structures. Owing to their superior strength-to-weight ratio, hybrid structures are excellent for energy absorption and have been extensively used in such engineering structures as automobiles, aircraft, military facilities,

M. Y. Huang · H. T. Hu
Department of Civil Engineering, National Cheng Kung University, Taiwan, Republic of China

Y.-S. Tai (✉)
Department of Civil Engineering, ROC Military Academy, Taiwan, Republic of China
e-mail: ystai@cc.cma.edu.tw

bridge structures and others. As a result, several researchers have recently addressed metal tubes that wrapped with a fiber-reinforced plastic composite. Various experimental and theoretical studies of the behaviors of different material and hybrid tubes have been carried out [1–13]. The theoretical model developed by Alexander [1] for calculating the average crushing force of a cylindrical tube under static axial crush is well known. Based on Alexander's classical solution, Hanefi and Wierzbicki [2] proposed a simplified analytical model of the static crushing of externally reinforced metal tubes, which agrees closely with experimental data. Huang and Wang [3] proposed a two-layer finite element model of the static axial collapse of carbon-reinforced composite tubes. The numerical simulation can effectively model the bevel trigger, representing the energy absorption characteristics and crushing failure mode of the composite specimens.

Han et al. [4] numerically studied hybrid composite unidirectional pultruded tubes that are over-wrapped with ±45° braided fiber-reinforced plastic, to elucidate their crushing behavior and energy absorbing capacity. Parametric investigations of the effects of the length of the tube, the thickness and type of braid, and the loading conditions on the crushing behavior of the tubes have been examined. Hage et al. [5] developed a finite element model based on modified Chang-Chang failure criteria to elucidate the quasi-static axial crush behavior of square aluminum-composite hybrid tubes. They also explored the effects of adhesion, friction between the aluminum tubes overwrapping with composite and verified their numerical model using experimental data.

Most previous studies of the crushing behavior of fiber-reinforced metal tubes were purely experimental. In this investigation, numerical simulations are carried out using the explicit non-linear finite element commercial software LS-DYNA and the results are compared with theoretical predictions to study how to establish an effective model for predicting the energy absorption behavior of hybrid tubes. The purpose is to develop a numerical method for evaluating the static and dynamic behavior of fiber-reinforced metal tubes under axial load. The effects of composite thickness, stacking orientations and material property of composite are also emphasized.

2 Theoretical Background

When tube is subject to an impact load, the governing equations for both bodies are:

Equation of mass conservation:

$$\rho V = \rho_0 \tag{1}$$

where V represents the relative volume; ρ denotes the current density, and ρ_0 denotes the reference density.

Equation of momentum conservation:

$$\sigma_{ij,j} + \rho f_i = \rho \ddot{u}_i \tag{2}$$

where σ_{ij} represents the Cauchy stress; f_i represents the body force density, and $\ddot{u}_i$ denotes the acceleration.

Equation of energy conservation:

$$\dot{E} = V s_{ij} \dot{\varepsilon}_{ij} - (p + q)\dot{V} \tag{3}$$

where s_{ij} and p denote the deviatoric stresses and hydrostatic pressure, respectively, as given in

$$s_{ij} = \sigma_{ij} + (p+q)\delta_{ij} \tag{4}$$

where q represents the bulk viscosity; δ_{ij} denotes the Kronecker delta (δ_{ij}=1, if i=j; otherwise δ_{ij}=0), and $\dot{\varepsilon}_{ij}$ denotes the strain rate tensor.

$$p = -\frac{1}{3}\sigma_{ij}\delta_{ij} - q = -\frac{1}{3}\sigma_{kk} - q \tag{5}$$

Based on the virtual work principle, Eq. 2 can be expressed as a weak form of equilibrium equation

$$\int_v \left(\rho\ddot{u}_i - \sigma_{ij,j} - \rho f\right)\delta u_i dv + \int \left(\sigma_{ij}n_j - t_i\right)\delta u_i ds + \int \left(\sigma_{ij}^{+} - \sigma_{ij}^{-}\right)n_j\delta u_i ds = 0 \tag{6}$$

where δu_i fulfills all boundary conditions, and the integrations are over the current geometry. Application of the divergence theorem gives

$$\int_v \left(\sigma_{ij}\delta u_i\right)_{,j} dv = \int \sigma_{ij}n_j\delta u_i ds + \int \left(\sigma_{ij}^{+} - \sigma_{ij}^{-}\right)n_j\delta u_i ds \tag{7}$$

and noting that

$$\left(\sigma_{ij}\delta u_i\right)_{,j} \sigma_{ij,j}\delta u_i = \sigma_{ij}\delta u_{i,j} \tag{8}$$

leads to the weak form of the equilibrium equations:

$$\delta\pi = \int_v \rho\ddot{u}_i\delta u_i dv + \int_v \sigma_{ij}\delta u_{i,j} dv - \int_v \rho f_i\delta u_i dv - \int t_i\delta u_i ds = 0 \tag{9}$$

If the finite element technique is interconnected using a matrix form, Eq. 9 becomes

$$\sum_{m=1}^{n}\left\{\int_{v_m} \rho N^t N a dv + \int_{v_m} B^t\sigma dv - \int_{v_m} \rho N^t b dv - \int_{\partial b_1} N^t t ds\right\}^m = 0 \tag{10}$$

where N is an interpolation matrix, σ is the stress vector, B is the strain–displacement matrix, a is the nodal acceleration vector, b is the body force load vector, and t are applied traction loads. The equation is integrated in time and is applied to evaluate the equation of state and for a global energy balance

3 Numerical Simulations

3.1 Description of Analysis Model

All numerical simulations were conducted using the commercial finite element program LS-DYNA [14]. Steel-composite hybrid tubes were geometrically modeled as two-layer cylindrical shells, as displayed in Fig. 1. The dimensions of the extruded metal tube in all of the models were L=170 mm, D=58 mm and t=1.0 mm, and composite wall thicknesses of 0.5, 0.8 and 1.0 mm were considered.

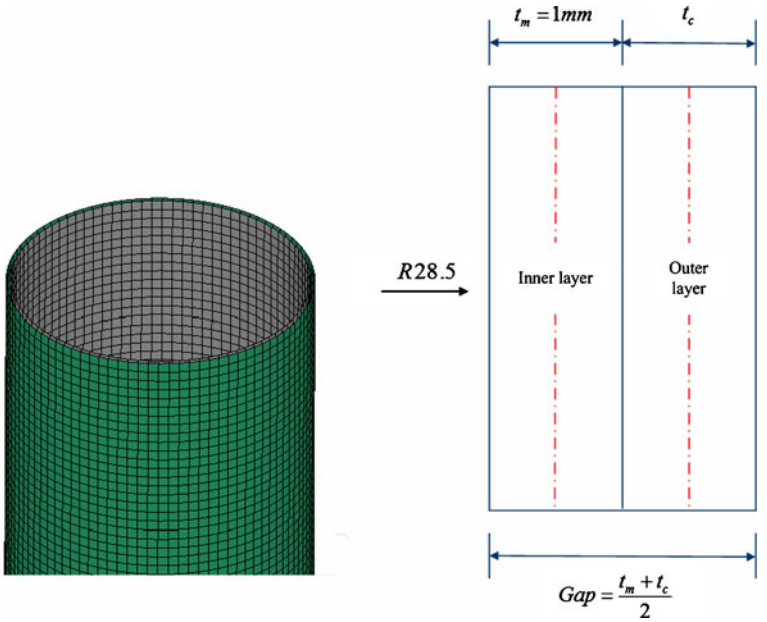

(a) modelling of the tube (b) Cross section of compound tube wall

Fig. 1 Two-layer finite element model of steel-composite compound tube

Both steel and composite tubes were modeled using Belytschko-Tsay four-node shell elements and a mesh size of 2.0 mm. The elements formed a lumped mass matrix, as required by the explicit calculation scheme, and were therefore suitable for analyzing large deformations. The steel and composite mid-planes were separated by a small gap that equaled the average thickness of the two walls (Fig. 1) and the stiffness-type hourglass control model was adopted to eliminate the zero-energy modes. The steel tube was modeled using three integration points through the thickness and one integration point in the element plane. Additionally, the different layers with certain stacking orientations were defined using integration points of the composite each of which represented one stacking lay-up.

In the modeling of quasi-static crushing, to reduce the number of time steps and thereby the computational burden, the mass density of both tubes is scaled up by multiplying the original density by a factor of 1000, to ensure that quasi-static loading is modeled during the simulation. The dynamic tests were performed by moving an impacting mass of 117 kg at a velocity of 10 m/s to assess the crushing behavior.

A simulation was carried out using a whole model because of uncertainty in the destruction pattern. In all simulations of axial crushing, the bottom end of the tube was assumed to be built-in and is constrained in all degrees of freedom. The upper end was free and compressed by rigid loading plate that moved at a downward initial velocity.

In the quasi-static and dynamic crushing simulations of interaction between steel and composite walls, the three contact algorithms were applied to avoid interpenetration during the movement and progressive folding.To simulate the interaction between the steel and the composite overwrap, the friction coefficient between all of the contact surfaces was set to 0.2. One of contact algorithms was a self-contact algorithm to prevent interpenetration during the deformation of the tubes by the command “contact_automatic_single_surface”. The deletion of failed elements during the crushing process caused the erosion of the inner

and outer layers. To prevent self-penetration within the inner layer and the outer layer, the contact interface of "contact_eroding_single_surface" was selected. Moreover, to simulate the bonding between the steel layer and the outer layer of the composite tube, the contact interface "contact_tiebrack_nodes_only" was used to account for the action of both normal and shear forces on the interface surface, according to the tiebreak criterion; both forces were assumed to be 100 N.

3.2 Mechanical Characteristics of Material

The metal tubes in this study were made of high-strength steel, which is a strain rate-sensitive material with a Young's modulus E=195 GPa, density=7850kg/m_3 and yield stress σ_0= 495 MPa. To yield accurate numerical results, Fig. 2 plots the stress–strain curves for various strain rates that were used in the numerical simulation. They were obtained by performing dynamic tensile tests using a Hopkinson Split Bar. Table 1 presents the mechanical properties of the composite tube, which were taken from the literature [3, 5].

3.3 Failure Criteria for Composite Layers

Composite material model 54"mat_enhanced_composite_damage"of LS-DYNA that was selected for our analysis was the most effective model of the composite material. The user can input arbitrary properties of the orthotropic materials, and unidirectional layers in composite shell structures can be defined. Either the Tsai-Wu failure criteria or the Chang-Chang failure criteria for each lamina can be applied. The Chang-Chang failure criteria modified the Hashin failure criteria to account for the non-linear shear stress–strain behavior, and the post-failure degradation was defined, enabling the behavior of the laminate to be analyzed after the failure of each successive lamina. This model applies four failure criteria. The following equations represent the failure criteria.

(a) In tensile fiber mode, E_a,E_b,G_{ab},ν_{ab},ν_{ba} are reduced to zero after lamina failure.

$$\sigma_{aa} > 0 \ \ then \ \ e_f^2 = \left(\frac{\sigma_{aa}}{X_t}\right)^2 + \beta\left(\frac{\sigma_{ab}}{S_c}\right) - 1 \begin{cases} \geq 0 \ failed \\ < 0 \ elastic \end{cases} \tag{11}$$

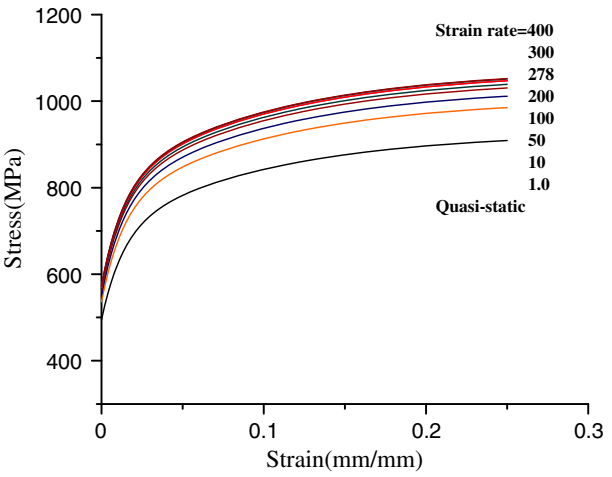

Fig. 2 Stress-plastic strain curves at various strain rates

Table 1 Mechanical properties of unidirectional carbon/BMI resin lamina and E-glass/epoxy

Properity	Description	Value(Carbon)	Value(Glass)
ρ	Density	1.53 g/cm^3	1.80 g/cm^3
E_a	Longitudinal modulus (fiber direction)	135 Gpa	30.9 Gpa
E_b	Transverse modulus (perpendicular to fiber)	9.12 Gpa	8.3 Gpa
G_{ab}	In-plane shear modulus (ab plane)	5.67 Gpa	2.8 Gpa
ν ba	Minor poisson's ratio	0.021	0.0866
X_t	Longitudinal tension strength (fiber direction)	2326 Mpa	798 Mpa
X_c	Longitudinal compressive strength (fiber direction)	1236 Mpa	480 Mpa
Y_t	Transverse tension strength (perpendicular to fiber)	51 Mpa	40 Mpa
Y_c	Transverse compressive strength (perpendicular to fiber)	209 Mpa	140 Mpa
S_c	In-plane shear strength	87.9 Mpa	70 Mpa

(b) Compressive fiber mode causes fiber buckling. Hence, the parameters $E_a, \nu_{ab}, \nu_{ba} = 0$

$$\sigma_{aa} < 0 \ \ then \ \ e_c^2 = \left(\frac{\sigma_{aa}}{X_c}\right)^2 - 1 \begin{cases} \geq 0 \ failed \\ < 0 \ elastic \end{cases} \tag{12}$$

(c) When the matrix begins to crack, the enters the tensile matrix mode, causing the values of E_b, ν_{ba}, G_{ab} to be zero.

$$\sigma_{bb} > 0 \ \ then \ \ e_m^2 = \left(\frac{\sigma_{bb}}{Y_t}\right)^2 + \beta\left(\frac{\sigma_{ab}}{S_c}\right) - 1 \begin{cases} \geq 0 \ failed \\ < 0 \ elastic \end{cases} \tag{13}$$

(d) When the lamina fails, the material constants $E_b, G_{ab}, \nu_{ab}, \nu_{ba}$ are set to zero. Accordingly, the failure mode is called the compressive matrix mode.

$$\sigma_{bb} < 0 \ \ then \ \ e_d^2 = \left(\frac{\sigma_{bb}}{2S_c}\right)^2 + \left[\left(\frac{Y_c}{2S_c}\right)^2 - 1\right]\left(\frac{\sigma_{bb}}{Y_c}\right) + \left(\frac{\sigma_{ab}}{S_c}\right)^2 - 1 \begin{cases} \geq 0 \ failed \\ < 0 \ elastic \end{cases} \tag{14}$$

In Equations 11–14, σ_{aa} is the stress in the fiber direction, σ_{bb} is the stress perpendicular to fiber direction and σ_{ab} is the shear stress in the lamina plane. ν_{ab} and ν_{ba} are the major and minor Poisson's ratio, respectively.

4 Results and Discussion

A number of indicators of crashworthiness are typically determined for crush components to evaluate their performance and compare it with that of other energy absorbing systems. The mean crushing force (P_m) and mass-specific energy absorption (E_s) are the primary parameters selected to evaluate the energy that can be absorbed by hybrid tubes. Generally, collapse involves plastic buckling and the formation of progressive folds. The formation of these folds causes the characteristic fluctuation in the axial force. Therefore, the mean

crushing force in this investigation was defined as the average of the axial crushing force following the peak force (Fig. 3), and the mass-specific energy absorption is defined as,

$$E_s = \frac{E_{total}}{\Delta M} = \frac{E}{A\Delta L\rho} \tag{15}$$

where ΔM denotes the mass in the crushing length of the cylindrical tube; E_{total} is the total energy that is absorbed in the crushing process; ΔL represents the effective crushing length; ρ is density, and A is the cross-sectional area of the cylindrical tube.

4.1 Comparison with Previous Analytical Models

Cylindrical metal tubes that are externally wrapped with composites with three thicknesses under static crushing were simulated and the material mechanical properties in Table 1 were utilized to obtain the theoretical prediction using Eqs. A10 and A17 (Appendix). Figure 4 and Table 2 compare the numerical and analytical results. Figure 4 plots of mean force as a function of thickness of the composite. All of the predicted values in the work of Wang and Lu [6] exceeded those of in the work of Hanefi and Wierzbicki [2]. The simulated values are closer to the predictions based on Eq. A17 in reference [6]. The percentage error between the simulated and predicted results was highest when the composite wall had a thickness of 0.5 mm, and declined as the thickness of the composite increased. Even though a thickness of 0.5 mm was associated with a large error, the mean force at thicknesses of 0.8 and 1.0 mm were simulated with satisfactory accuracy, and the predicted and simulated results matched accurately. This result demonstrates that the developed finite element model yields satisfactory approximations to the theoretically predicted values.

4.2 Influence of Wall Thickness and Loading Condition

The simulation results show in Tables 3 and 4 and Figs. 5, 6, 7, 8 and 9. Figure 5 plots force-deformation cures, which reveal that oscillations are followed by a high initial peak load. Since composite has a high strength to weight ratio, the figure indicates that the application of the composite significantly increases the crushing load, and the fiber-reinforced metal tubes exhibit excellent crashworthy performance.

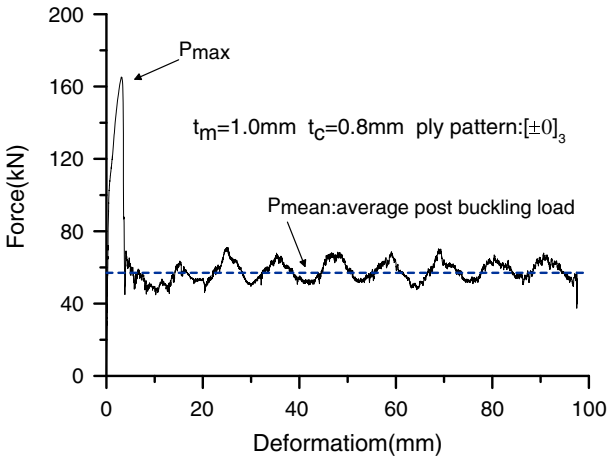

Fig. 3 Axial mean crushing force

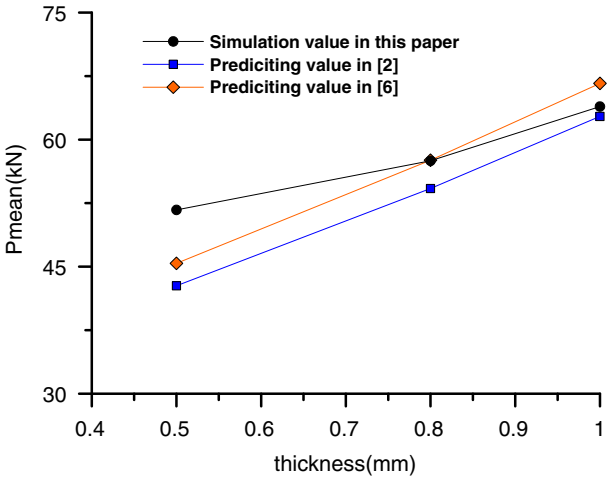

Fig. 4 Comparison between numerical simulation and analytical values of P_m calculated in reference [2] and [6]

Composites of three thicknesses (0.5, 0.8, 1.0 mm) were used to overwrap the steel tubes to form hybrid tubes. Figures 6 and 7 present the modeled results, which reveal that composite overwraps can be applied to enhance effectively the crushing characteristics and energy absorbing capacity of the tubes. As expected, increasing the thickness of the composite increased the mean crushing force. The mean crushing loads of the hybrid tubes were approximately 22.39, 44.53 and 62.69% higher than the corresponding values for the metal tubes, respectively (Fig. 7). Figure 8 plots the crushing force against the crushing deformation. The dynamic and static results are identical in that they both reveal progressive failures, with only slight differences in the force-displacement curves. Comparing the static and dynamic crushing results demonstrates that although the folding patterns were very similar, increasing the impact velocity gives increased the force. Figure 9 indicates that the specific energy absorption increases with the thickness of the composite wall. Moreover, the figure shows that the responses in the static and dynamic tests were close to each other, for increasing the thickness. Apparently, the three composite wall thicknesses were insufficient to constrain the external movement of the metal tube. Therefore, the metal compound tube exhibited the properties of both steel and composite material. For this reason, the specific energy absorption increased gradually with a change in thickness of the composite.

4.3 Effect of Ply Orientation

Figures 10, 11 and 12 present composites of a particular thickness (0.8 mm) with different stacking sequences subject to quasi-static and dynamic crushing loading, to elucidate the

Table 2 Comparison between simulation results and the theoretical prediction values in reference [2] and [6]

t_c (mm)	Simulation value of P_m in this study	Predicting value of P_m from Eq. A10 in reference [2]	Predicting value of P_m from Eq. A17 in reference [6]	Error between prediction data in reference [2] and simulation value in this paper	Error between prediction data in reference [6] and simulation value in this paper
0.5	51.70	42.74	45.38	17.33	12.22
0.8	57.50	54.22	57.56	5.70	0.10
1	63.90	62.74	66.64	1.82	4.29

Table 3 Summary of crushing characteristics of metal and composite compound tubes under static loading

Description of model				Simulation results							
Material property	t_m (mm)	t_c (mm)	Ply pattern	Pmax (kN)	Pm (kN)	E_m(J)	E_c(J)	E_t(J)	E_s(J/kg)	Deformation(mm)	Energy increase(%)
Bare mental	1.0	–	–	101.50	40.20	3967.80	–	3967.80	18.77	97.66	–
Carbon fiber	1.0	1.0	$[\pm0]_3$	174.60	65.40	5181.70	1125.20	6306.90	26.37	97.51	58.95
	1.0	0.8	$[\pm0]_3$	165.25	58.10	4978.50	847.26	5825.76	23.65	97.50	46.83
	1.0	0.5	$[\pm0]_3$	147.14	49.20	4684.10	491.96	5176.06	20.61	98.10	30.45
	1.0	0.8	$[\pm15]_3$	151.64	58.40	4877.20	935.33	5812.53	23.45	98.11	46.49
	1.0	0.8	$[\pm30]_3$	130.37	50.20	4004.20	948.51	4952.71	20.10	97.52	24.82
	1.0	0.8	$[\pm45]_3$	133.70	49.10	3726.90	1120.20	4847.10	19.58	98.00	22.16
	1.0	0.8	$[\pm60]_3$	137.28	53.50	3834.70	1403.90	5238.60	21.10	98.28	32.03
	1.0	0.8	$[\pm75]_3$	133.79	49.00	3871.50	939.90	4811.40	19.50	97.69	21.26
	1.0	0.8	$[\pm90]_3$	112.79	42.20	4031.10	128.44	4159.54	16.88	97.56	4.83
Glass fiber	1.0	0.8	$[\pm0]_3$	133.68	46.70	4111.90	524.02	4635.52	18.77	97.75	16.83
	1.0	0.8	$[\pm15]_3$	132.63	45.80	4085.60	534.67	4620.15	18.68	97.91	16.44
	1.0	0.8	$[\pm30]_3$	121.05	45.70	4023.20	587.87	4609.82	18.61	98.03	16.18
	1.0	0.8	$[\pm45]_3$	119.21	45.70	3932.80	634.63	4567.41	18.51	97.68	15.11
	1.0	0.8	$[\pm60]_3$	121.74	45.90	3873.10	691.93	4565.03	18.53	97.51	15.05
	1.0	0.8	$[\pm75]_3$	118.43	45.50	3974.40	619.12	4593.17	18.64	97.53	15.76
	1.0	0.8	$[\pm90]_3$	119.11	41.40	3984.40	190.03	4174.25	16.85	98.05	5.20

E_m and E_c represenr the energy absorption of metal and composite, respectively.

E_t is the total energy absorbed in the crushing process

Table 4 Summary of crushing characteristics of metal and carbon composite compound tubes under dynamic loading

Description of model				Simulation results						
Loading condition	t_m (mm)	t_c (mm)	Ply pattern	Pmax (kN)	Pm (kN)	E_m(J)	E_c(J)	E_t(J)	E_s(J/kg)	Deformation(mm)
Dynamic(V=10 m/s)	1.0	–	–	103.14	44.30	5803.00	–	5803.00	19.78	135.55
	1.0	0.5	$[\pm 0]_3$	154.61	56.60	5161.10	524.69	5685.79	22.28	99.70
	1.0	0.8	$[\pm 0]_3$	172.37	59.70	4902.50	790.54	5693.04	24.89	90.52
	1.0	1	$[\pm 0]_3$	180.71	63.10	4760.80	933.02	5693.82	27.22	85.29
	1.0	0.8	$[\pm 15]_3$	156.98	54.10	4872.90	875.27	5748.17	22.78	99.86
	1.0	0.8	$[\pm 30]_3$	138.17	51.10	4699.50	1086.80	5786.30	21.22	107.96
	1.0	0.8	$[\pm 45]_3$	150.47	54.40	4489.20	1281.30	5770.50	21.17	107.92
	1.0	0.8	$[\pm 60]_3$	177.73	56.90	4227.30	1496.20	5723.50	22.39	101.20
	1.0	0.8	$[\pm 75]_3$	173.83	52.20	4627.20	1094.10	5787.50	20.95	108.11
	1.0	0.8	$[\pm 90]_3$	184.36	45.30	5596.20	191.30	5693.04	18.09	126.65

E_m and E_c represenr the energy absorption of metal and composite, respectively.

E_t is the total energy absorbed in the crushing process

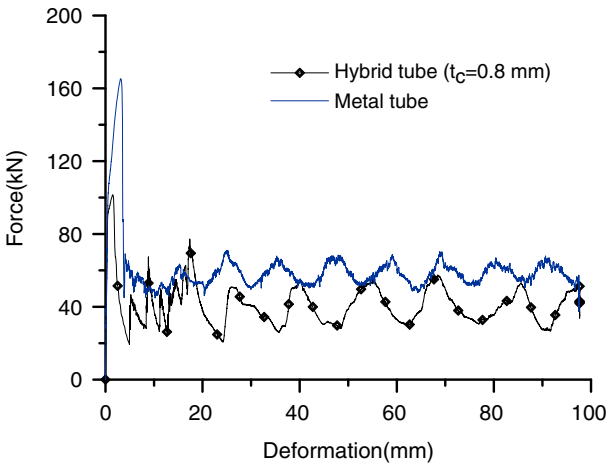

Fig. 5 Force-deformation curve of compound tube and bare metal tube subject to quasi-static crushing

effect of the ply pattern on the energy absorption of the compound tubes. Figure 10 indicates that the values of E_s and P_{mean} under dynamic loading exceed that under the quasi-static condition except when the ply orientation is $[\pm 15°]_3$. This result reveals that each ply is really not having a higher energy absorbing capacity under dynamic impact loading than under the quasi-static condition. Since the different ply patterns are associated with different energy absorption mechanisms of, as the winding angle increases to $[\pm 60°]_3$, the composite layer contributes increasingly to the energy absorption in the folding process and both loading conditions yields more similar results (Fig. 11). However, even though the energy absorption capacity of the composite observably increases, the compound tube with the $[\pm 60°]_3$ ply pattern is really not the best energy absorber. In fact, the $[\pm 0°]_3$ compound tube exhibits the highest energy absorption capacity; although the contribution of its composite layer to that capacity is lower, because of the deformation mode.

To study further the behavior of the hybrid tubes under axial deformation, Fig. 12 plots their deformation profiles. As the winding angle exceeds 30, the concertina mode of the metal was replaced by a diamond mode. The energy efficiency in this axisymmetric mode is better than that of the asymmetric mode. Hence, as a side effect, the $[\pm 0°]_3$ compound tube has high energy absorption. When the metal tube exhibits an asymmetric collapse mode, the

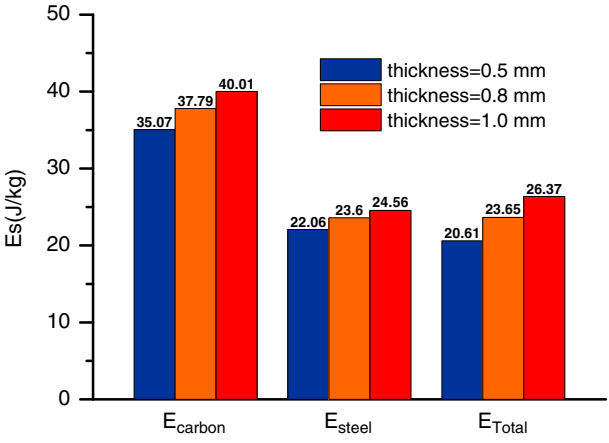

Fig. 6 Effect of thickness of composite on Es

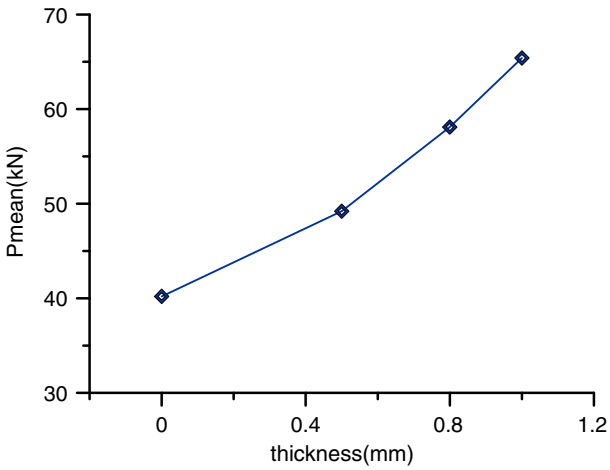

Fig. 7 Effect of composite wall thickness on P_m

high energy absorption of the composite layer effectively results in a high energy absorption capacity of the hybrid tube. Accordingly, the energy efficiency of the composite plays an important role. The above analysis remarkably indicates that the energy absorption capacity depends strongly on the deformation mode of the metal tube and fiber-reinforcement does not affect the collapse failure mode of the metal. It also indicates that composite overwraps can effectively improve the crushing characteristics and energy absorbing.

4.4 Effect of Composite Property

Figure 13 illustrates the force-deformation curves of the carbon and glass fiber-reinforced metal tubes with $[\pm 0°]_3$ stacking orientation. The crushing responses of the compound tubes with 0.8 mm-thick carbon or glass composite demonstrate that the metal tube that is wrapped in carbon fiber enhances the crushing capacity a much more remarkably than that offered by the glass fiber. With respect to the first crushing force, the carbon fiber has the highest force-carrying capacity. However, the crushing force of the carbon fiber-reinforced

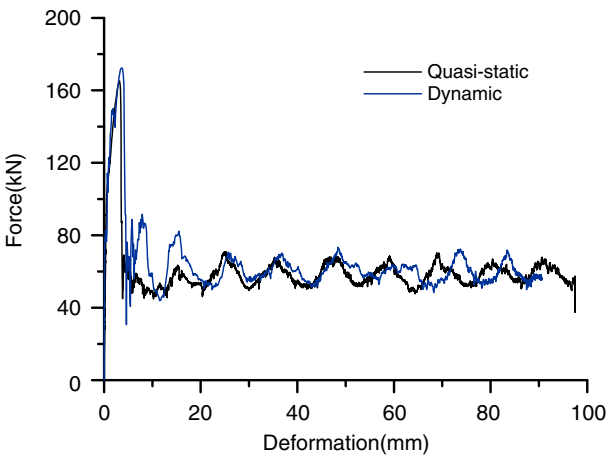

Fig. 8 Comparison of responses of force-deformation history curves to static and dynamic impacts

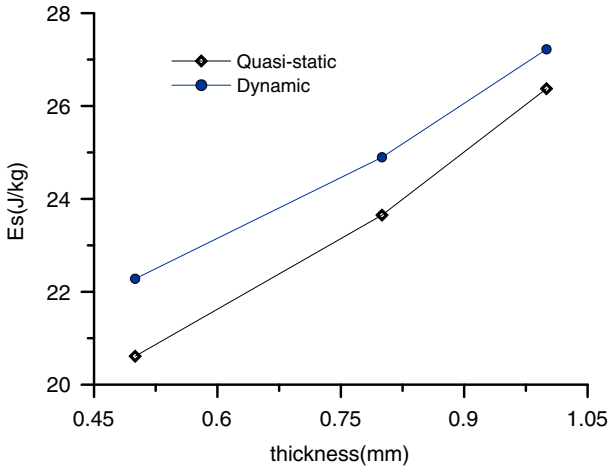

Fig. 9 Comparison of effect of composite wall thickness on energy absorption capacity in static tests with that in dynamic tests

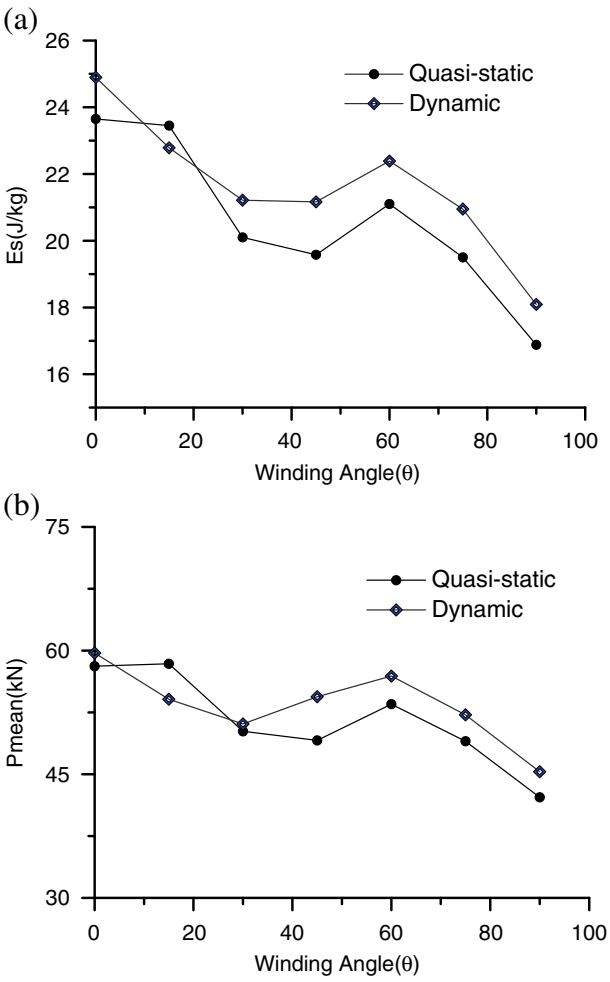

Fig. 10 $[\pm\theta]_3$ stacked fiber-reinforced metal tubes (**a**) Energy absorption capacity (**b**) mean crushing force

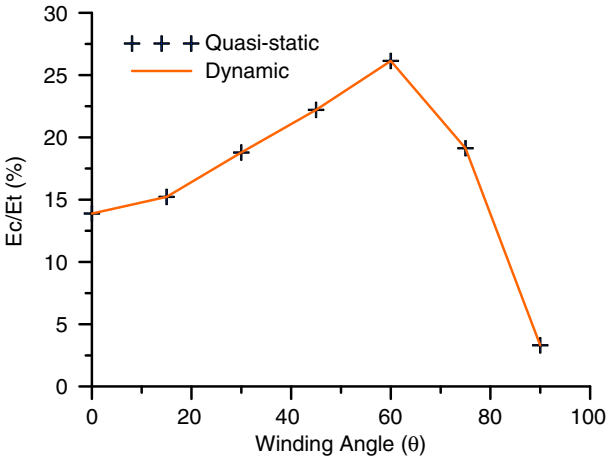

Fig. 11 Contribution of composite in $[\pm\theta]_3$ stacked fiber-reinforced metal tubes

metal tube also increases after the first peak crushing load is reached. Notably, the crushing force efficiency, defined as the ratio of the mean crushing load to the largest mean crushing load is 0.352 and 0.349 for the carbon and glass fiber, respectively. These values show that the hybrid tube with carbon fiber has a higher energy absorbing efficiency than the tube that is wrapped glass fiber.

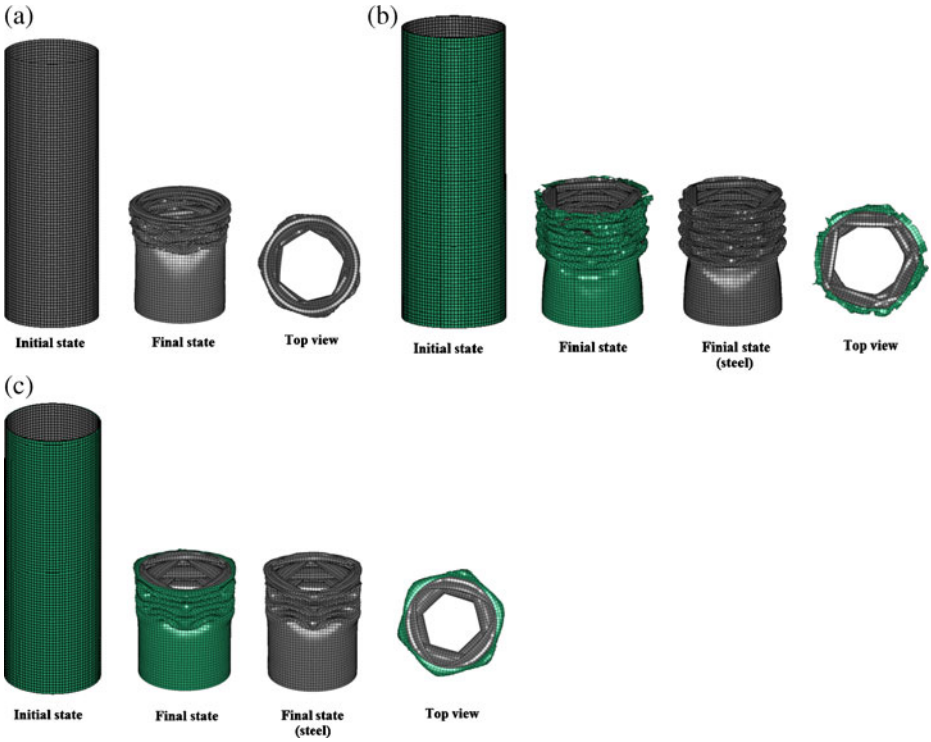

Fig. 12 Numerical models of deformation under static loading; **a** Metal tube, **b** Compound tube with $[\pm0]_3$ ply pattern, **c** Compound tube with $[\pm30]_3$ ply pattern

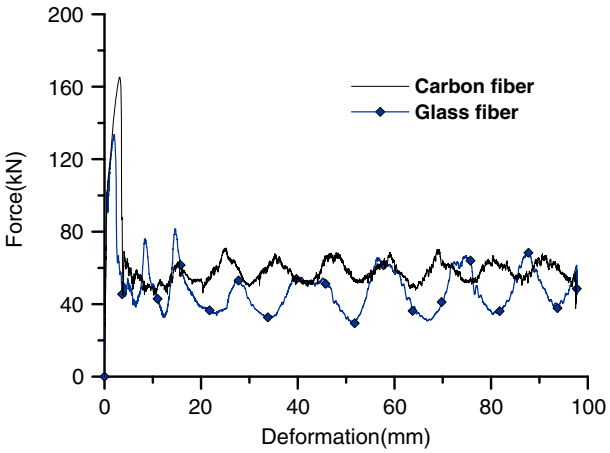

Fig. 13 Force-deformation curves of compound tubes that are wrapped with carbon and glass fibers with $[\pm 0°]_3$ ply pattern

Based on the results in Fig. 14, neither fiber-reinforced metal tube exhibited a regular variation of the energy absorbing efficiency with the stacking orientation. The carbon fiber hybrid tubes produced a higher energy absorption capacity than the glass fiber for each ply pattern, whereas Es of the glass fiber varies slightly with the ply pattern. In the case of $[\pm 90°]_3$, both materials respond similarly and substantially to variations in the ply pattern at $[\pm 0°]_3$ and $[\pm 15°]_3$. The $[\pm 0°]_3$ stacked fiber-reinforced metal tubes have the highest Es. As summarized in Table 3, carbon fiber improved the energy absorption capacity by 46.83%, whereas the glass fiber increased it by 16.83%. The results indicate that the compound tubes depend mainly on the tensile and compressive strength associated with the longitudinal and biaxial modulus of the materials. Accordingly, the selection of the composite material is important in ensuring favorable energy absorption capacity.

5 Conclusion

The static and dynamic axial crushing behavior and energy absorption efficiency of metal tubes that are wrapped with composite were studied by including the effect of the strain rate on the metal layer. Overwrapping the metal tubes with composite is an

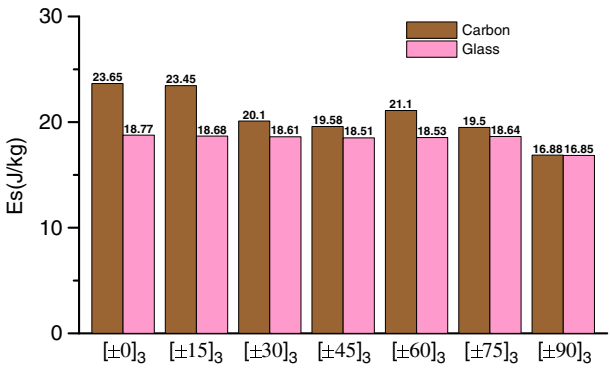

Fig. 14 Energy absorption capacities of compound tubes with various material properties of composite and stacking sequences, subject to quasi-static crushing

effective means of increasing energy absorption capacity and the improving the crushing characteristics of such tubes. Energy absorption efficiency is examined as a function of composite wall thickness, loading condition, fiber ply orientation and composite property.

Simulations results are consistent with theoretical predictions. The results in this investigation reveal that the compound tubes undergo stable progressive failure in both quasi-static and dynamic crushing tests. A comparison of composites of various thicknesses demonstrates that the specific energy absorption in dynamic and static tests was an increasing function increased with the thickness of the composite wall. The stacking sequence significantly affects the energy absorption capacity. The $[\pm 0°]_3$ compound tube had the highest energy absorption efficiency of all tubes with the same thickness of composite. Notably, the collapse mode is an effective indicator of the energy absorption mechanism and the composite material property is also an important factor in determining energy absorption efficiency.

Appendix: Analytical Model

Based on Alexander's model of metal tubes, Hanefi and Wierzbicki [2] proposed a simplified analytical model of the static compression of externally composite-reinforced metal tubes, with an angle of orientation of the overwrap from the tube axis of 0° (Fig. A1). Consider the crushing mechanism of five stationary plastic hinges that produces a folding that is composed of four elements of equal lengths. According to the model, when the composite walls are under tension at the outward fold, the glass fibers do not contribute to the resistance of the composite material. Accordingly, at hinge lines 2 and 4, the contribution of the composite wall is negligible, and the resisting bending moment of the metal walls is given by

$$M_0^{(2)} = M_0^{(4)} = \frac{\sigma_0 t_m^2}{4} \tag{A1}$$

where σ_0 and t_m are the yield strength and wall thickness of metal, respectively.

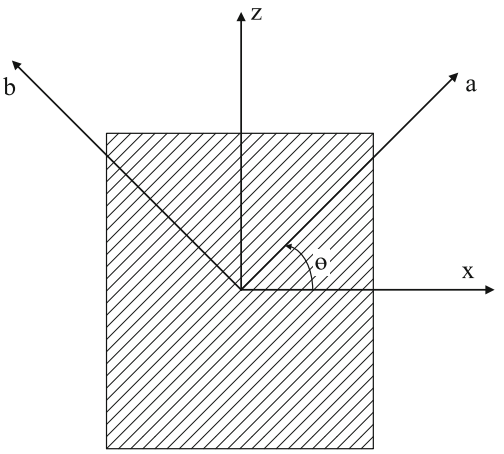

Fig. A1 Material coordinate system for a fiber reinforced lamina in which a is the fiber direction and b is the transverse direction

Similarly, at hinge line 3, when the composite walls are under compression at the inward fold, the bending moment of the bi-material section is given by Eq. A2. The mean of the bending moments calculated using Eqs. A1 and A2 yields Eq. A3.

$$M_0^{(3)} = \frac{\sigma_0 t_m^2}{4}\left[1 + 2\left(\frac{\sigma_{cr}}{\sigma_0}\right)\left(\frac{t_c}{t_m}\right) + 2\left(\frac{\sigma_{cr}}{\sigma_0}\right)\left(\frac{t_c}{t_m}\right)^2 - \left(\frac{\sigma_{cr}}{\sigma_0}\right)^2\left(\frac{t_c}{t_m}\right)^2\right] \tag{A2}$$

$$M_0 = C\frac{\sigma_0 t_m^2}{4} \tag{A3}$$

$$C = \frac{1}{2}\left[2 + 2\left(\frac{\sigma_{cr}}{\sigma_0}\right)\left(\frac{t_c}{t_m}\right) + 2\left(\frac{\sigma_{cr}}{\sigma_0}\right)\left(\frac{t_c}{t_m}\right)^2 - \left(\frac{\sigma_{cr}}{\sigma_0}\right)^2\left(\frac{t_c}{t_m}\right)^2\right] \tag{A4}$$

σ_{cr} is the ultimate stress of composite in compression perpendicular to fiber direction, t_c is the wall thickness of composite.

Furthermore, to satisfy the Tresca yield criteria, the contribution of the metal shell to the membrane energy and the bending energy that is dissipated in the wall of the hybrid tube must be

$$W_b = 2\pi^2 aC\sigma_0 t_m^2 \tag{A5}$$

and

$$W_m = r\pi\sigma_0 t_m H^2 \tag{A6}$$

where a is initial radius of tube and H is the hinge length.

During the formation of a fold, when the composite is under tension, the contribution of the composite to the membrane energy consists of two parts with the interface between the fractured and unfractured of the composite. Simplification yields the energy absorbed by the composite reinforcement in tension and compression, given by Eqs. A7 and A8, respectively.

$$(W_c)_{ten} = 2\pi a t_c E_c\left[\int_0^{w_{ct}}\left(\frac{s}{a}\right)^2 ds + \int_{w_{ct}}^{H} {\varepsilon_{ct}}^2 ds\right] = 2\pi a t_c E_c {\varepsilon_{ct}}^2 H \tag{A7}$$

$$(W_c)_{com} = 2\pi a t_c \int_0^{2H} \sigma_{cf}\frac{s}{a} ds = 2\pi t_c \sigma_{cf} H^2 \tag{A8}$$

Accordingly,

$$W_c = (W_c)_{ten} + (W_c)_{com} = 2\pi t_c H(H\sigma_{cf} + aE_c{\varepsilon_{ct}}^2) \tag{A9}$$

where σ_{cf} and ε_{ct} are, respectively, the ultimate stress of composite in compression in fiber direction and strain limits of composite in tension in fiber direction, E_c is Young's modulus of composite in tension in fiber direction, w_{ct} is the length of unfractured composite parts and the interface between the fractured and unfractured parts is denoted by $s = w_{ct}$.

The external work equals the internal energy dissipated for a given crushing distance. Abramowicz [13] developed an approximate expression for the actual compression length

of metal columns and determined an effective crushing length. Finally, the crushing load P_m is obtained:

$$P_m = \frac{1}{3.44H - 2t}\left(2\pi^2 a\sigma_0 C{t_m}^2 + 4\pi t\sigma_{eq}H^2 + 2\pi a t_c E_c{\varepsilon_{ct}}^2 H\right) \tag{A10}$$

$$\sigma_{eq} = (\sigma_0 t_m + \frac{1}{2}\sigma_{cf} t_c)/t \tag{A11}$$

However, considering the mechanism of crumpling of hybrid tubes that was proposed by Hanefi and Wierzbicki [2], Wang and Lu [6] considered the deformation of both radial inward and outward folds. In calculating the bending energy, they assumed that the metal tubes obeyed the Von Mises yield criterion and considered the resistance of the fiber-reinforced layer to tensile bending deformation. Hence, they derived the three contributory terms and a formula for P_m that differed from that of Hanefi and Wierzbicki [2], as follows.

$$W_b = \frac{4}{\sqrt{3}}\pi^2 a\sigma_0 t_m^2 C_0 + \frac{2}{\sqrt{3}}\pi\sigma_0 {t_m}^2 H C_1 \tag{A12}$$

$$C_0 = 1 + \left(\frac{\sigma_{cxc} + \sigma_{cxt}}{\sigma_0}\right)\left(\frac{t_c}{t_m}\right) + \left(\frac{\sigma_{cxc} + \sigma_{cxt}}{\sigma_0}\right)\left(\frac{t_c}{t_m}\right)^2 - 0.5\left(\frac{{\sigma_{cxc}}^2 + {\sigma_{cxt}}^2}{{\sigma_0}^2}\right)^2\left(\frac{t_c}{t_m}\right)^2 \tag{A13}$$

$$C_1 = \left(\frac{\sigma_{cxc} + \sigma_{cxt}}{\sigma_0}\right)\left(\frac{t_c}{t_m}\right) + \left(\frac{\sigma_{cxt} + \sigma_{cxc}}{\sigma_0}\right)\left(\frac{t_c}{t_m}\right)^2 - 0.5\left(\frac{{\sigma_{cxt}}^2 - {\sigma_{cxc}}^2}{{\sigma_0}^2}\right)^2\left(\frac{t_c}{t_m}\right)^2 \tag{A14}$$

$$W_m = 2\pi\sigma_0 t_m H^2 + 2\pi H^2 t_m \sigma_0 \tag{A15}$$

$$W_c = \frac{2}{3}\pi a^2 t_c \sigma_{ct}{\varepsilon_{ct}}^2 + 2\pi H^2 t_c \sigma_{cc} \tag{A16}$$

$$P_m = \frac{1}{3.44H - 2t}\left(4\pi t\sigma_{eq}H^2 + \frac{2}{\sqrt{3}}\pi\sigma_0 {t_m}^2 C_1 H + \frac{4}{\sqrt{3}}a\pi^2\sigma_0 {t_m}^2 C_0 + \frac{2}{3}\pi a^2 t_c \sigma_{ct}{\varepsilon_{ct}}^2\right) \tag{A17}$$

where σ_{cxc} and σ_{cxt} are axial compressive strength and axial tensile strength of the fiber-reinforced layer, respectively, σ_{cc} is critical stress in the fiber direction subjected to compression and σ_{ct} is critical stress in the fiber direction subjected to tension.

References

1. Alexander, J.M.: An approximate analysis of the collapse of thin cylindrical shells under axial loading. Q J Mech Appl Math **13**(1), 10–15 (1960)
2. Hanefi, E.H., Wierzbicki, T.: Axial crush resistance and energy absorption of externally reinforced metal tubes. Compos. Part B Eng. **27**(5), 387–394 (1996)
3. Huang, J., Wang, X.: Numerical and experimental investigations on the axial crushing response of composite tubes. Compos. Struct. **91**(2), 222–228 (2009)

4. Han, H., Taheri, F., Pegg, N., Lu, Y.: A numerical study on the axial crushing response of hybrid pultraded and ±45° braided tubes. Compos. Struct. **80**(2), 253–264 (2007)
5. EI-Hage, H., Mallick, P.K., Zamani, N.: Numerical modeling of quasi-static axial crush of square aluminum-composite hybrid tubes. Int. J. Crashworthiness. **9**(6), 653–664 (2004)
6. Wang, X., Lu, G.: Axial crushing force of externally fibre-reinforced metal tubes. Proc. IMechE J. Mech. Eng. Sci. **216**(9), 863–874 (2002)
7. Farley, G.L., Jones, R.M.: Crushing characteristics of continuous fiber-reinforced composite tubes. J. Compos. Mater. **26**(1), 37–50 (1992)
8. Al, E.I., Afizun, A.: Crushing behavior of pultruded composites. J. Mekanikal **24**, 15–31 (2007)
9. Mamalis, A.G., Manolakos, D.E., Ioannidis, M.B., Papapostolou, D.P.: The static and dynamic axial collapse of CFRP square tubes: finite element modelling. Compos. Struct. **74**(2), 213–225 (2006)
10. Bambach, M.R.: Axial capacity and crushing of thin-walled metal, fibre-epoxy and composite metal-fibre tubes. Thin Wall Struct. **48**(6), 440–452 (2010)
11. Mamalis, A.G., Manolakos, D.E., Ioannidis, M.B., Kostazos, P.K., Papapostolou, D.P.: Axial collapse of hybrid square sandwich composite tubular components with corrugated core: numerical modelling. Compos. Struct. **58**(4), 571–582 (2002)
12. Guillow, S.R., Lu, G., Grzebieta, R.H.: Quasi-static axial compression of thin-walled circular aluminium tubes. Int. J. Mech. Sci. **43**(9), 2103–2123 (2001)
13. Abramowicz, W.: The effective crushing distance in axially compressed thin walled metal columns. Int. J. Impact. Eng. **1**(3), 309–317 (1983)
14. LS-DYNA Theoretical Manual, V.971, Livermore Software Technology Corporation, Livermore, CA, USA (2006)